Nanoscale Advances

PAPER

Cite this: *Nanoscale Adv.*, 2025, 7, 3396

Directing the adsorption and assembly of laponite nano-discs at oil–water interfaces †

Sohaib Mohammed, [a] Ahmed W. Alsmaeil, [b] Hassnain Asgar, [a] Prince Ochonma, [b] Antonios Kouloumpis, [c] Yang Jia, [a] Rituparna Hazra, [a] Ivan Kuzmenko, [d] Emmanuel P. Giannelis [c] and Greeshma Gadikota [*ab]

Achieving tunable controls on the adsorption and self-assembly of nanoscale building blocks at immiscible fluid interfaces is essential for synthesizing advanced materials, stabilizing emulsions, and the sustainable storage and recovery of fluids. Although extensive efforts have been directed toward resolving the assembly of spherical nanoparticles at water–hydrocarbon interfaces, 2D nanoparticles have received far less attention. In this study, we developed novel controls to direct the adsorption and assembly of 2D laponite nano-discs (diameter = ~30 nm and thickness = ~1 nm) at water–heptane interfaces using traces of sodium dodecyl sulfate (SDS) surfactant, demonstrated by advanced *in situ* small-angle X-ray scattering, atomic force microscopy, spinning drop tensiometer measurements and molecular dynamics simulations. The results show that SDS surfactant displaces the adsorbed laponite nano-discs from the interface toward the aqueous phase. The extent of this displacement increases with SDS concentration such that high SDS concentrations convert laponite-rich interfaces to SDS-rich interfaces free of laponite nano-discs. This transformation is associated with significant alterations in the rheological and nanomechanical properties of the host interface. In this context, reduction in interfacial tension and interfacial stiffness and an increase in the interfacial deformation is observed on increasing the SDS concentration from 0 to 0.1 wt%. The displacement of laponite nano-discs from the interface is driven by strong electrostatic interactions between the hydrophilic SDS group and interfacial water molecules. These studies unlock new insights into the adsorption and assembly of 2D nanoscale particles at water–hydrocarbons interfaces that are relevant for various applications related to energy and environmental science and engineering.

Received 17th February 2025
Accepted 1st April 2025

DOI: 10.1039/d5na00160a

rsc.li/nanoscale-advances

1. Introduction

Immiscible liquids interfaces (particularly water–hydrocarbon interfaces) are ubiquitous in nature and highly relevant to a wide spectrum of energetic,[1] environmental,[2] biological,[3] and chemical applications.[4] Laponite-stabilized emulsions play a key role in enhanced oil recovery (EOR) and high-temperature foam stability, where their ability to reinforce interfacial viscoelasticity improves the performance of foam-based mobility control techniques in steam injection processes.[5] Additionally, laponite nano-discs are widely explored in biomedical applications, including drug delivery, bioimaging, and tissue engineering, due to their high biocompatibility and tunable surface properties.[6,7] Their strong adsorption at interfaces also makes them valuable in Pickering emulsions, which are utilized in cosmetics, pharmaceuticals, and food formulations.[8] These diverse applications underscore the importance of understanding the interfacial mechanics of laponite nano-discs, as studied in our work. In this context, these interfaces have been used as a template for directing the assembly and transport of symmetric and asymmetric inorganic and metal nanoparticles,[9–15] opening a new pathway for synthesis of advanced materials with unique and tunable nanoscopic properties.[16,17] Hence, developing informed controls on the rheology, nanomechanical properties and energetics of water–hydrocarbon interfaces enables predictive adsorption, assembly, and transport of the nanoscale building blocks of the assemblies at the interfaces. However, it is still unclear how to

[a] School of Civil and Environmental Engineering, College of Engineering, Cornell University, Ithaca, NY 14853, USA. E-mail: gg464@cornell.edu; Tel: +1 608-262-0365
[b] Department of Chemical and Biomolecular Engineering, College of Engineering, Cornell University, Ithaca, NY 14853, USA
[c] Department of Materials Science and Engineering, College of Engineering, Cornell University, Ithaca, NY 14853, USA
[d] X-Ray Science Division, Advanced Photon Source, Argonne National Laboratory, Lemont, Illinois 60439, USA

† Electronic supplementary information (ESI) available: Description of the optimization of laponite unit cells using the density functional theory approach, characterizing the bulk laponite suspensions and probing the average dimensions of suspended laponite nanoparticles using disc-like models on the scattering curves and the AFM measurements and analysis approach of the interfacial stiffness and deformation and intermolecular interactions. See DOI: https://doi.org/10.1039/d5na00160a

link the directed adsorption and assembly of potential nanoparticles with unique shapes to the chemical and physical nature of water–hydrocarbon interfaces.

Particular attention has been directed toward understanding the self-assembly of symmetric 3D spherical nanoparticles at water–oil interfaces.[18–20] Significant insights have been gained

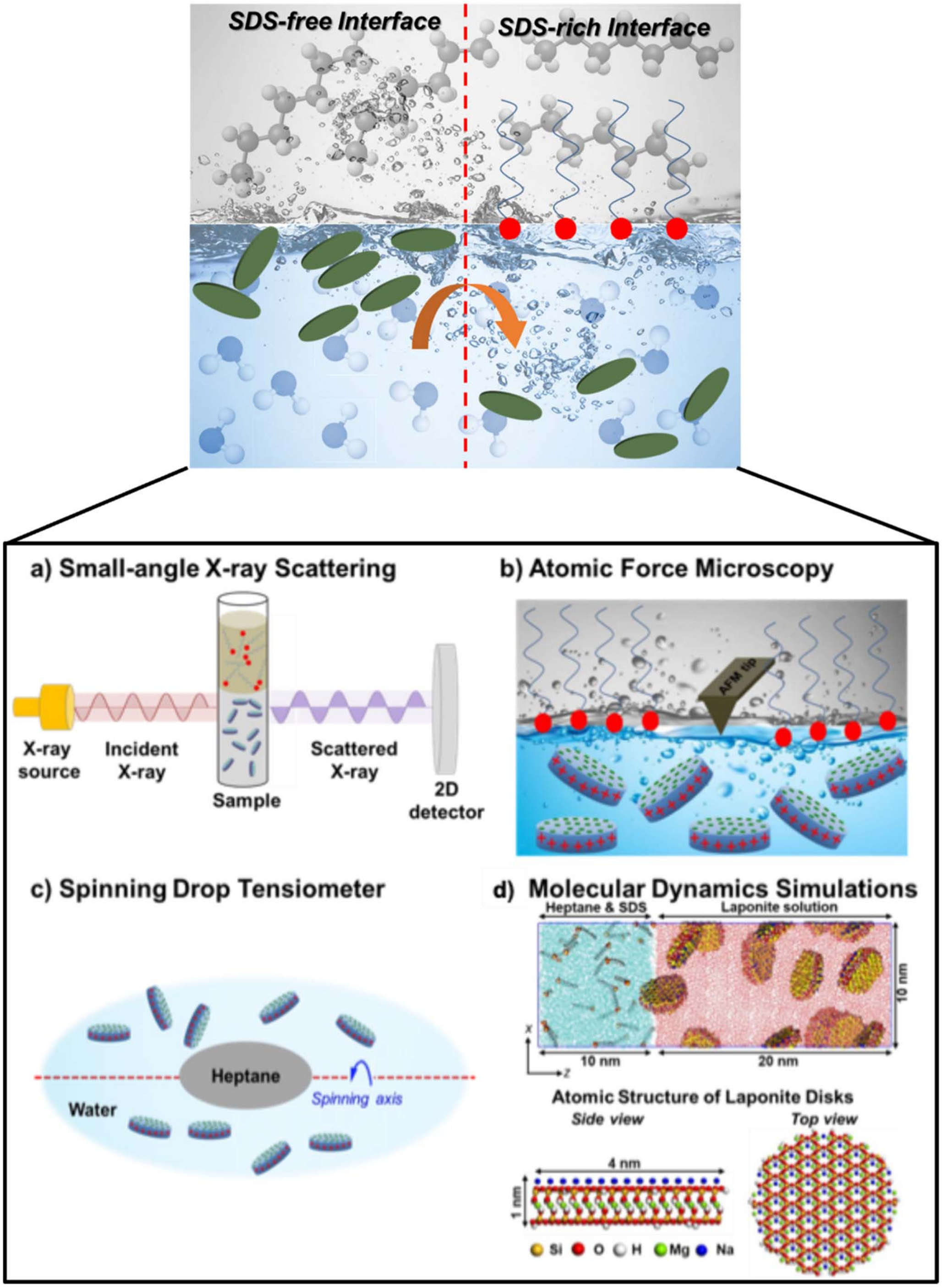

Fig. 1 Schematic representation of the scientific phenomenon of the displacement of laponite nano-discs in presence of SDS from the water–heptane interface investigated in this study along with: (a) the experimental setup for the ultrasmall/small-angle X-ray scattering (USAXS/SAXS) measurements of laponite nanoparticles at the water–heptane interface; (b) the experimental setup of atomic force microscopy measurements of water–heptane interfaces; (c) the spinning drop tensiometer setup used to measure the interfacial tension and dilatational modulus of water–heptane interfaces; (d) the simulated initial configurations show the suspended LAPONITE® nano-discs in the water phase and the dissolved SDS molecules in the heptane phase. The atoms of the water and heptane are shown in lines, while laponite nanoparticles and SDS molecules are shown in VDW drawing methods implemented in VMD software. Bottom snapshots show the side and top views of the atomic structures and dimensions of laponite discs used in the MD simulations.

regarding the interfacial structure, transport, and self-assembly of various inorganic and metallic nanoparticles and the effect of interfacial properties in driving their assembly. The driving force of the nanoparticle assembly at the interfaces is the reduction in the excess free energy resulting from the decrease in the contact area between the two bulk phases as the nanoparticles occupy the interfaces.[21] Further, the self-assembly at liquid–liquid interfaces is also influenced by the size and shape of the individual nanoparticle, with larger nanoparticles preferentially occupying the interface.[22,23] Moreover, the surface properties and concentrations of spherical nanoparticles directly affect the morphology and the packing of the self-assembled nanoparticles at liquid–liquid interfaces.[24] Although these insights are crucial to control the adsorption and assembly of spherical nanoparticles at water–hydrocarbon interfaces, it is still unclear whether these findings are applicable to 2D nanoparticles. Hence, a detailed study is needed to elucidate the adsorption and assembly of 2D nanoparticles model at water–hydrocarbon interfaces.

Laponite is a 2D disc-like synthetic clay that exhibits distinctive self-assembled structures at the liquid–liquid interfaces.[25] It has been extensively used in pharmaceutical, cosmetics and biomedical applications[26–28] and to stabilize water–oil emulsions.[29–32] laponite nano-discs tend to adsorb and assemble at water–hydrocarbon interfaces, inducing a reduction in the interfacial tension[33] and zeta potential,[34] increase in the viscosity of the continuous phase and provide a physical barrier to coalescence.[35] Further, chemically modified amphiphilic laponite nano-discs show surfactant-like behavior at interfaces. In this context, laponite particles tethered with hydrophobic C_{18} chains,[33] short chain aliphatic amines,[29] alanine[36] and hexylamine[37] demonstrated enhanced emulsion stability. Despite these advances in understanding the structural and transport behavior of interfacial 2D laponite nano-dicks, innovative ways to direct the adsorption and assembly of these nanoparticles at water–hydrocarbon interfaces are lacking. Further, enabling predictive controls on the interfacial rheology and nanomechanics on reversing the adsorption and assembly of interfacial nano-discs are still missing.

Nanoparticle size also dictates interfacial energy balance and adsorption kinetics. Machrafi *et al.* (2022) showed that larger nanoparticles influence interfacial energy more significantly, altering surface tension.[38] Smits *et al.* (2019) found that smaller nanoparticles are more easily displaced by surfactants, while larger ones exhibit stronger adsorption stability.[39] Our observations align with these findings, where our results demonstrate that larger nanoparticles exhibit stronger interfacial stability, resisting surfactant-induced desorption, while smaller nanoparticles show increased displacement at higher surfactant concentrations. Additionally, we observed that elongated nanoparticles tend to alter local surfactant distributions, affecting interfacial stabilization. Shape also plays a role in adsorption. Barbul *et al.* (2018) demonstrated that non-spherical nanoparticles experience asymmetric adsorption forces,[40] impacting interfacial behavior. Machrafi *et al.* (2022) suggested that anisotropic nanoparticles modify surfactant competition at interfaces.[38] Our study confirms that shape anisotropy influences adsorption dynamics, which we aim to explore further.

To direct the adsorption and assembly of 2D laponite nano-discs at the water–oil interface and to link this directed adsorption and assembly to the properties of the host interface, we focus on the sodium dodecyl sulfate (SDS)-driven adsorption of interfacial laponite nano-discs at water–heptane interfaces using low surfactant concentrations (≤0.1 wt%) dissolved in the heptane phase. We have previously shown that SDS surfactant can effectively reverse the adsorption of spherical silica nanoparticles (dia. 50 nm and 100 nm) at water–heptane and water–toluene interfaces.[41] Here, we applied *in situ* Ultrasmall –/Small-Angle X-ray Scattering (USAXS/SAXS), atomic force microscopy (AFM), spinning drop tensiometer (SDT) measurements and classical molecular dynamics (MD) simulations to probe the effect of interfacial SDS molecules on the adsorption and assembly of 2D laponite nano-discs at water–heptane interfaces (see Fig. 1). Advanced modeling and analysis approaches are used to determine the spatial and temporal evolution of interfacial 2D laponite nanoparticles in the presence of different SDS concentrations.

2. Methods

2.1 Sample preparation

Suspensions of 2D laponite nano-discs (diameter = ∼30 nm and thickness = ∼1 nm) in deionized water with a concentration of 10 mg mL^{-1} (1 wt%) are prepared by mixing the laponite powder with water under 800 rpm for 1 hour at ambient temperature. Laponite powder of XLG grade was purchased from BYK Additives & Instruments. Heptane-bearing SDS solutions are prepared by dissolving 0.001, 0.01 and 0.1 wt% SDS powder in pure heptane under 800 rpm for 1 hour at ambient temperature. To prepare the SDS solutions, we distinguished between two different conditions: (1) "heptane-free SDS solution," referring to SDS dissolved directly in ultrapure water without exposure to heptane, and (2) "heptane-bearing SDS solution," where SDS is introduced into the aqueous phase that has been in equilibrium with heptane to ensure controlled interfacial conditions. This distinction was made to investigate the impact of heptane on SDS adsorption and subsequent interfacial transformations. The formed interfaces are characterized using USAXS/SAXS, AFM and SDT measurements. Interfaces used for X-ray measurements are prepared by injecting 100 μL of the suspension into a glass tube of 5 mm diameter followed by injecting 100 μL of heptane-free and heptane-bearing SDS solutions, while interfaces for AFM and SDT measurements are prepared with lower volumes.

2.2 Ultra-small/small-angle X-ray scattering measurements

Operando USAXS/SAXS measurements on the laponite nanoparticles at water–heptane interfaces are performed at sector 9-ID-C at the Advanced Photon Source (APS), Argonne National Laboratory.[42,43] The data acquisition times for USAXS and SAXS measurements are 90 s and 5 s, respectively. USAXS and SAXS data are collected using a Bonse-Hart camera and a pinhole camera, respectively, on a Pilatus 100 K detector (Dectris Ltd., Baden Switzerland). The 2D USAXS and SAXS scattering are reduced and converted to 1D curves using the Nika[44] and Irena[45] macros written in Igor software. The background scattering from the empty glass tube is collected and subtracted from the scattering data. The X-ray flux at the sample is 10^{17} photon mm^{-2} s^{-1} while the applied energy is 21.0 keV (corresponding to a wavelength of 0.589 Å). The sample-to-detector distances (and geometry) are calibrated using silver behenate calibrant. Once the interface is identified, USAXS and SAXS data are collected from the interfacial region for about 60 minutes to capture the time-dependent assembly and adsorption of the 2D laponite nano-discs at the interfaces (see Fig. 1(a)).

2.3 Atomic force microscopy measurements

AFM measurements are conducted in peak force tapping mode on a Multimode 8, Nanoscope 6, using Peakforce-HIRS-F-A cantilevers (see Fig. 1(b)). A fluid cell is used for water–heptane emulsion measurements and the force–separation curves are obtained with a force of 7 nN, in all systems. The deflection sensitivity of the photodetector is calibrated by acquiring approach–retract curves on a sapphire sample in heptane and the spring constant of the cantilever is calibrated using the thermal method. A small droplet of the laponite aqueous solution is placed on the silicon wafer, and a larger drop of heptane with or without SDS added is placed in a way to completely cover the water droplet.

2.4 Interfacial tension measurements

The alterations in the rheological properties of water–heptane emulsions induced by laponite nano-discs and the SDS surfactant are characterized by measuring the interfacial tension and the corresponding dilatational modulus. A spinning drop tensiometer (SDT) is used to probe the interfacial tension of water–heptane emulsions in the presence and absence of laponite nano-discs as a function of SDS concentration (see Fig. 1(c)). The drop shape is fitted using the Young–Laplace model[46] and the interfacial tension is calculated using the ADVANCE software. The dilatational modulus (E) is obtained from the change in the interfacial tension (γ) and the droplet surface area (A) using $E = A\frac{d\gamma}{dA}$.[47] The oscillation amplitude is kept at 1000 rpm to ensure minimal changes in the droplet surface area.

2.5 Molecular dynamics simulations

Classical MD simulations are performed to capture the adsorption and assembly of 2D laponite nanoparticles at water–heptane interfaces and to provide molecular-level insights into the adsorption behavior, interaction forces, and structural organization of laponite nano-discs and SDS. 2D laponite nano-discs with a diameter of 4 nm and a thickness of about 1 nm are constructed from a validated and optimized unit cell (see Fig. 1(d)).[48,49] The unit cell is optimized using the density functional theory approach to ensure equilibrated laponite structure (see Fig. S1†). The optimized unit cell is replicated in x and y directions and the edges are cleaved to create the nano-disc (see Fig. 1(d)). The suspended nanoparticles phase is created by dissolving 10 nanoparticles in 58 157 water molecules in a cell of 10 nm × 10 nm × 20 nm length in x, y, z directions, respectively. The cell was extended further by 10 nm in the z-direction and solvated with the 3100 heptane molecules to form the water–hydrocarbons interface (see Fig. 1(d)). 0, 0.001, 0.01 and 0.1 wt% of SDS solutions are created by adding the corresponding number of SDS molecules. The intermolecular and intramolecular interactions of laponite nano-discs, water, heptane and SDS molecules are modeled using CLAYFF,[50] SPC/E,[51] and OPLSAA[52] forcefields, respectively.

The positions of the initially randomly distributed molecules and nanoparticles are optimized using the "steepest descent" method for 50 000 steps. The optimized configurations are equilibrated using semi-isotropic compression (NPAT) ensemble for 1 ns with compression in the z-direction only to keep the interfacial area (xy plane) constant. The output of the NPAT simulations step is equilibrated using NVT simulations for 100 ns followed by 50 ns NPAT production step. The temperature and pressure are kept at 298 K and 1 bar using Nose–Hoover thermostat[53,54] and Parrinello–Rahman barostat,[55] respectively. The equation of motion is integrated using leap-frog integrator with a time step of 1 fs. Short-range interactions are considered within 1.4 nm cutoff and long-range electrostatic interactions are calculated using Particle Mesh Ewald (PME) method.[56] MD simulations are conducted using GROMACS 2020.6 simulation package.[57]

3 Results and discussions

3.1 Interfacial structure of 2D laponite nano-discs

The interfacial structure of laponite nano-discs at water–heptane interfaces and in bulk water is resolved as a function of the SDS concentration using *in situ* USAXS/SAXS measurements collected for 60 minutes (see Fig. 2). USAXS/SAXS curves from laponite suspensions in bulk water confirm the disc-like geometry and the curves fitting demonstrate that the average dimensions of the laponite nano-discs are 34.67 ± 4.6 nm in diameter and 1.08 ± 0.06 nm in thickness (see Fig. S2†). The number and size distribution of bulk laponite nanoparticles is calculated by modeling the SAXS curves as nano-discs by incorporating the scattering contrast of laponite and water, the disc volume fractions, and the dimensions of the nano-discs. The obtained dimensions validate the model used to fit the USAXS/SAXS curves.

Interfacial laponite in SDS-free emulsions (*i.e.*, 0 wt% SDS) retain similar and time-independent scattering curves over 60 minutes. The identical scattering curves from the SDS-free interfaces indicate rapid laponite adsorption at the interface (t = 0 min), followed by high stability interfacial structures of the adsorbed nanoparticles. The rapid adsorption of laponite nanoparticles with high stability at the interfaces is also noted in the presence of 0.001 wt% and 0.01 wt% SDS (Fig. 2(b) and (c)). However, as the SDS concentration increases to 0.1 wt%, the scattering intensity from interfacial nano-discs decrease as time elapsed (Fig. 2(d)), suggesting a decrease in the interfacial

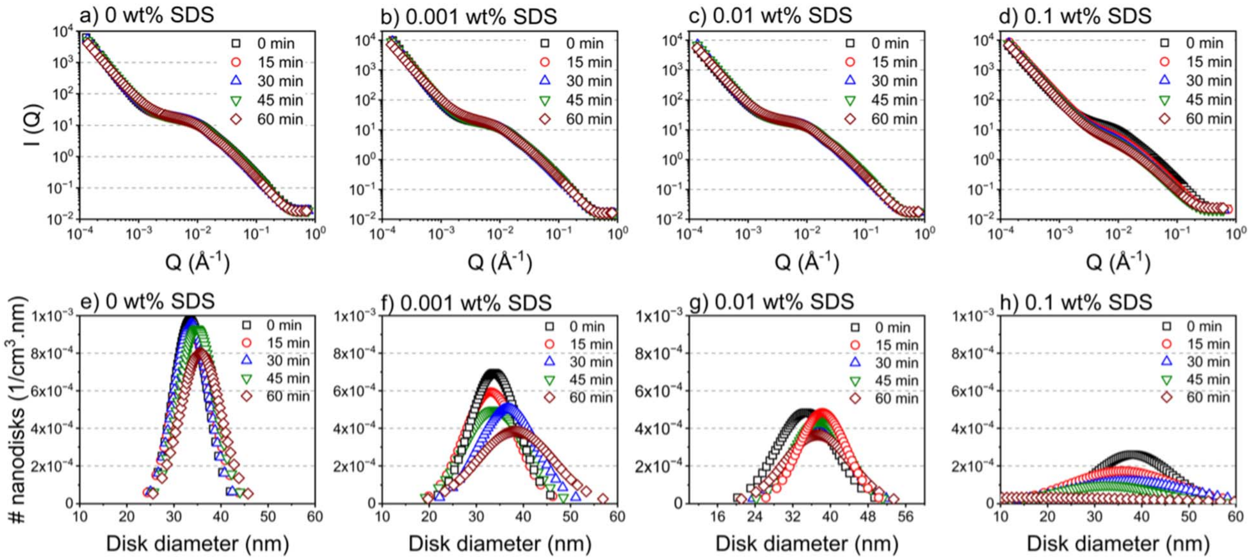

Fig. 2 Determination of the assembly of laponite discs as a function of SDS concentrations where (a–d) represent ultrasmall/small-angle X-ray scattering (USAXS/SAXS) intensity curves on the momentum transfer (Q) scale as a function of the dissolved SDS concentration and the elapsed measurement time, and (e–h) represent the number of laponite nano-discs as a function of the disc diameter, SDS concentration in the heptane phase and elapsed measurement time. The number of laponite nano-discs is obtained from modeling the scattering intensity curves as disc-like structures.

laponite scatterers as the surfactants occupy the interface. The decrease in the interfacial laponite scatterers leads us to hypothesize that SDS molecules displace laponite nano-discs from the interface toward the aqueous phase.

To verify this hypothesis, we calculated the number of interfacial laponite nano-discs as a function of their size distribution with different SDS concentrations dissolved in the heptane phase (Fig. 2(e–h)). The number of interfacial nano-discs shows slight decrease at SDS-free interface as time lapsed (Fig. 2(e)). As SDS molecules are added to the emulsion and start occupying the interface, the number of interfacial nanoparticles decreases systematically with the SDS concentration and as time elapsed. The slight decrease in the number of interfacial laponite nano-discs in the presence of 0.001 wt% and 0.01 wt% suggests that even small concentrations of interfacial SDS can displace interfacial laponite nano-discs toward the aqueous phase and the extent of this displacement increases as the interface is occupied by more SDS molecules. Interestingly, 0.1 wt% SDS displaces all laponite nanoparticles from the interface after 60 min, suggesting that the gradual migration of the dissolved SDS molecules in the bulk heptane toward the interface displaces the interfacial laponite nano-discs gradually toward the bulk region of the aqueous phase. The displacement of laponite nano-discs by interfacial SDS molecules is similar with the behavior of spherical silica nanoparticles with comparable sizes and concentrations at water–heptane and water–toluene interfaces.[41,58]

In SDS-free emulsions, the interface is dominated by laponite nano-discs that adsorb instantaneously on the interface. The interfacial laponite shows high stability with time, suggested by the number of interfacial particles probed by USAXS/SAXS measurements. Interfacial laponite nano-discs desorb from the interface and are displaced into the bulk aqueous phase as SDS molecules migrate from bulk heptane and start occupying the interfacial area. The magnitude of this displacement depends on the concentration of the SDS molecules present such that the interface becomes eventually laponite-free (and SDS-rich) at high SDS concentrations, leading to significant changes in the rheological and nanomechanical properties.

This displacement of interfacial laponite nano-discs from the interface is further analyzed by calculating the 2D number density maps, obtained from MD simulation trajectories (see Fig. 3). The 2D density maps are averaged over the xz plane during the last 10 ns of the simulation time to ensure equilibrated structures of interfacial and bulk laponite nano-discs. The 2D density maps show that the distribution of laponite nano-discs at the interfaces is highly affected by the SDS concentrations in heptane. An abundance of interconnected laponite nano-discs is observed at the interface of SDS-free emulsions. However, the adsorbed laponite nano-discs are systematically displaced from the interface toward the bulk aqueous phase as the SDS concentrations increased to 0.001 wt% and 0.1 wt%. Further, all the interfacial laponite nano-discs are desorbed and dispersed in the aqueous phase as the SDS concentrations in the heptane phase increase to 0.1 wt% (Fig. 3(d)). SDS-induced displacement of interfacial laponite nano-discs obtained from MD simulations is consistent with the observations from USAXS/SAXS measurements (Fig. 2).

Laponite nano-disc assemblies exhibit different configurations at the interface and in the bulk regions of SDS-free and SDS-bearing emulsions. Examples of these configurations are the stacked nano-discs (parallel orientation), house of cards

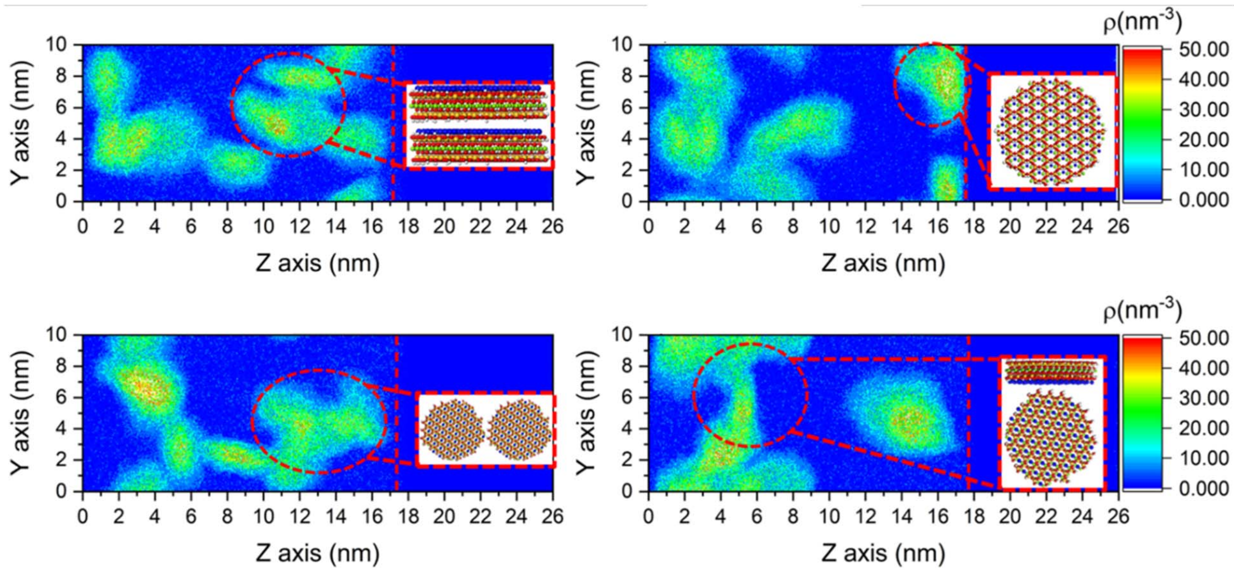

Fig. 3 Laponite assembly and orientation is determined using 2D density maps of SDS dissolved in the heptane phase. The 2D density maps are averaged over the last 10 ns of the simulation time to ensure equilibrated positions and configurations of laponite nano-discs. The insets show the assembly configurations and orientation of bulk and interfacial laponite nano-discs. Snapshots in panels a, c and d represent the stacked, overlapping and house of cards orientations, respectively.

(perpendicular orientation) and overlapping nano-discs orientation (Fig. 3). Further, individual nano-discs orient parallel to the interface such that it occupies a large area of the interface per interfacial laponite nano-discs at low SDS concentrations. The different configurations of laponite assemblies in the aqueous phase stem from unique charge distribution on the negatively charged faces and the positively charged edges of the laponite nano-discs.[59] These assemblies are consistent with Porod curves ($I(Q) \times Q^4$ *vs.* Q^4) obtained from the scattering measurements, whereas the power law slope of interfacial laponite is between 3 and 4 (see Fig. S3†), indicating surface fractal-like assemblies.[60–62]

3.2 Interfacial rheological and nanomechanical properties

The rheological and nanomechanical properties of water–heptane interface are characterized by measuring the interfacial tension, stiffness, and extent of deformation (Fig. 4). The interfacial tension of laponite-free emulsions decreased significantly from 39.11 ± 1.37 to 24.87 ± 0.74 mN m^{-1} on increasing the SDS concentration from 0 to 0.1 wt%, respectively. However, the presence of adsorbed laponite nano-discs at the interface induces significant changes and the interfacial tension is only slightly decreased from 36.14 ± 1 to 32.94 ± 0.5 mN m^{-1}, when the SDS concentration increases from 0 to 0.1 wt%, respectively. The relatively stable interfacial tension of water–heptane mixture in the presence of laponite nano-discs can be attributed to the aging effect of laponite solutions in which the viscosity of the aqueous phase increases with time and hinders significant changes in the interfacial rheology compared to laponite-free solutions.[63–66] The corresponding dilatational modulus,[67] defined as the change in the interfacial tension divided by the interfacial area variation, decreased on increasing the SDS concentration in the heptane phase. laponite-free emulsions showed first an increase in the dilatational modulus values on increasing the SDS concentration from 0 to 0.001 wt%, followed by a significant decrease to about 8.57 ± 1.75 mN m^{-1} for 0.1% SDS. However, when laponite is present a systematic decrease in the interfacial dilatational modulus from 42 ± 4 to 11.1 ± 1.52 mN m^{-1} for 0 and 0.1 wt% SDS, respectively, is seen. The SDS and laponite-driven changes in the interfacial tensions of water–heptane are consistent with previous experimental and computational studies of *n*-hexane–water and trichloroethylene–water systems.[68,69]

We next studied the nanomechanical properties of the interfaces (interfacial stiffness and deformation profiles) as a function of SDS concentration (see Fig. 4(b)) using force spectroscopy measurements. The interfacial stiffness and deformation are obtained from the force applied to the interface using an atomic force microscopy probe (see Fig. S4†).[70] The interfacial stiffness decreased minimally from 31 ± 1 mN m^{-1} to 28 ± 1 mN m^{-1} as the SDS concentration increased from 0 to 0.01 wt%, respectively, followed by a significant decrease to 21 ± 2 mN m^{-1} in the presence of 0.1 wt% SDS. Similarly, the corresponding interfacial deformation increased from 217 ± 7 nm to 224 ± 9 nm as the SDS concentration increased from 0 to 0.01 wt%, respectively, followed by a significant increase to 263 ± 19 nm as 0.1 wt% SDS is added to the emulsion. These trends in the nanomechanical properties suggest that SDS-rich interfaces are easier to deform compared to laponite-rich interfaces.

The evolution of SDS-rich interfaces driven by the adsorption and accumulation of SDS molecules at the interface is also evidenced by the local density profiles along the direction normal to the interface (z-axis), obtained from MD simulations (see Fig. 4(c)). SDS density profiles show peaks in the interfacial region with no indication of SDS molecules in bulk heptane,

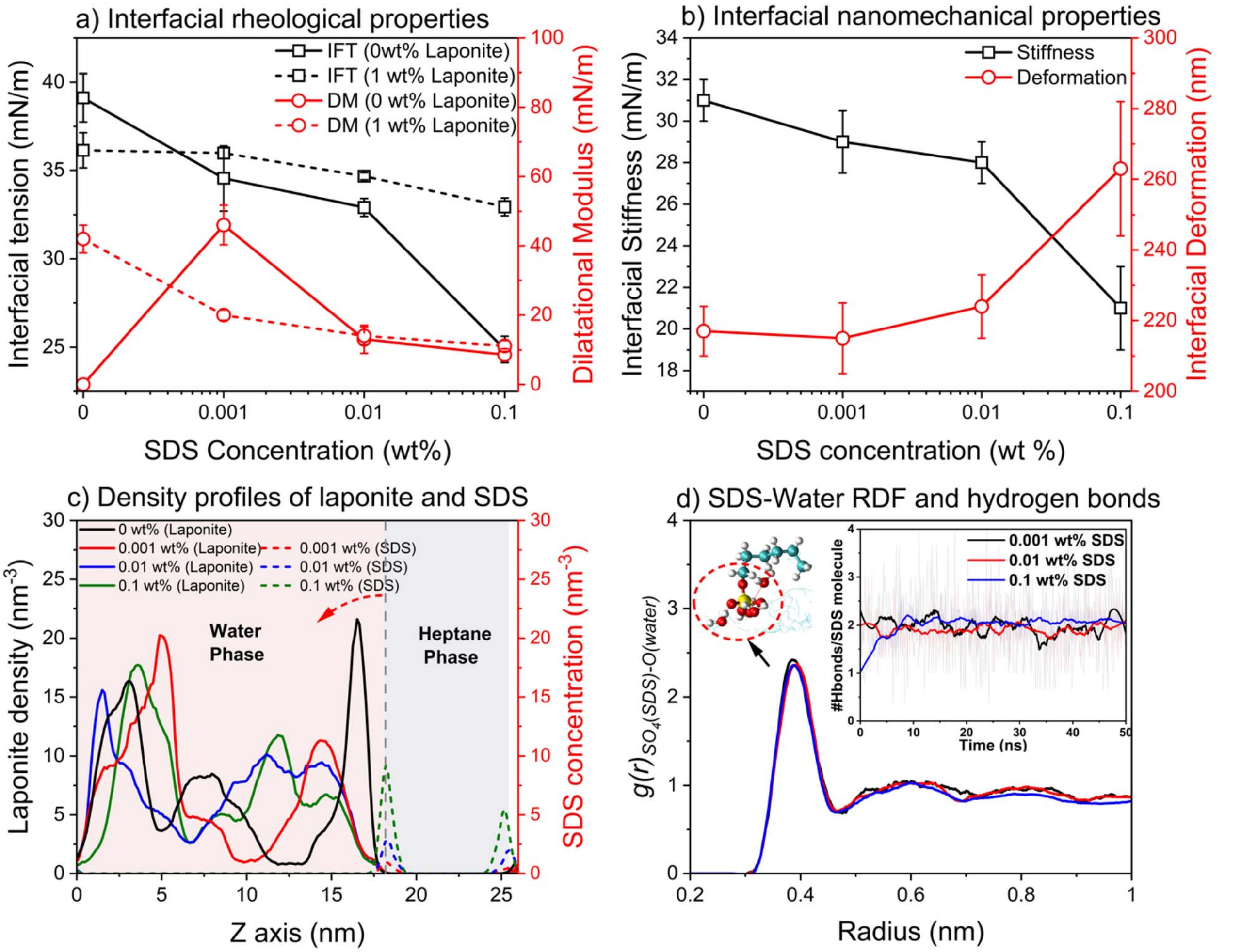

Fig. 4 (a) The interfacial tension and dilatational modulus of water–heptane interfaces in the presence and absence of 1 wt% laponite as a function of SDS concentration in heptane, are obtained from spinning drop tensiometer measurements. (b) The interfacial stiffness and deformation as a function of the SDS concentration are obtained from atomic force microscopy measurements. (c) The density profiles of laponite nano-discs and SDS molecules along the direction normal to the interface (*z*-axis) as a function of SDS concentration, are obtained from MD simulations. The density profiles are averaged over the last 10 ns of the simulation time. (d) The radial distribution function of the SO_4 group in the SDS molecule and oxygen atoms of water at different SDS concentrations averaged over the last 10 ns of the simulation time. The figures in inset show a snapshot of SDS–water interactions at the interface and the hydrogen bonding profile of SDS–water.

suggesting that all the dissolved molecules migrate to the interface. The adsorption of SDS molecules at the interface is associated with a decrease in the interfacial laponite density, due to the desorption of interfacial laponite particles back to the bulk aqueous phase. The systematic transition from laponite-rich to SDS-rich interfaces with the increase in SDS concentration drives the alterations in the interfacial rheological and nanomechanical properties.

The driving force of the transition from laponite-rich to SDS-rich interfaces is the preferential interaction of the SDS hydrophilic head with interfacial water molecules (see Fig. 4(d)). These interactions are characterized by the radial distribution function (RDF) and the number of hydrogen bonds between the sulfate group and interfacial water molecules. RDFs show a prominent peak corresponding to the first coordination shell of water molecules surrounding the hydrophilic SO_4 group.[71–73] Interestingly, the first coordination peak in the RDF profile does not change with the SDS concentration, suggesting a stable structure and density of the hydration water around the hydrophilic sulfate group of all the interfacial SDS molecules. This concentration-independent structure of sulfate hydration water is further confirmed by probing the dynamic hydrogen bonding between the hydrophilic group and interfacial water molecules normalized by the number of SDS molecules.[74] Hydrogen bonding profiles show that sulfate groups form about two hydrogen bonds with the surrounding water molecules at the interface. The interaction, orientation, and adsorption of SDS with interfacial water molecules drive the interfacial alterations including displacing the laponite nano-discs from the interface toward the aqueous phase.

Combining AFM, SDT and MD simulation, we notice that, without SDS, laponite nano-discs strongly adhere to the interface, forming a stable network. Introducing SDS reduces adhesion, with 0.1 wt% SDS fully displacing nano-discs into the aqueous phase, transforming the interface from laponite-rich to SDS-rich. The transition from a laponite-rich to SDS-rich interface alters interfacial tension, stiffness, and deformability. laponite nano-discs lower interfacial tension, but SDS gradually replaces them, softening the interface. AFM measurements show SDS disrupts the rigid laponite network, reducing stiffness at higher concentrations. Increased SDS concentrations enhance interfacial flexibility compared to laponite-stabilized interfaces. MD simulations confirm that laponite adsorption is driven by electrostatic and van der Waals forces (Section 4.3). SDS molecules preferentially interact with interfacial water, gradually displacing laponite nano-discs, consistent with AFM and SDT results. Radial distribution function (RDF) analysis shows strong SDS–water interactions, reinforcing their competitive adsorption.

The dilatational modulus reflects the mechanical response of the interfacial layer to dynamic perturbations, which directly influences the stability and rheological properties of emulsions. Our findings show that at low SDS concentrations, laponite nano-discs dominate the interface, forming a rigid structure with a high dilatational modulus that enhances interfacial elasticity, leading to higher bulk viscosity and improved emulsion stability. As SDS concentration increases, SDS molecules gradually displace laponite nano-discs from the interface, reducing the dilatational modulus and resulting in a more fluid-like interfacial layer with lower bulk viscosity and enhanced shear thinning behavior. At high SDS concentrations ($\geq$0.1 wt%), the interface becomes SDS-dominated with a minimal dilatational modulus, weakening the interfacial network and decreasing emulsion stability. This transition from a laponite-stabilized to an SDS-stabilized interface is well captured through dilatational modulus changes, mirroring the trends observed in bulk rheology. Our combined interfacial tension and rheological measurements provide a comprehensive picture of how laponite nano-discs and SDS modulate emulsion properties through interfacial mechanics.

3.3 Energetics of interfacial transitions

The intermolecular interactions driving the transition from laponite-rich to SDS-rich interfaces and the associated interfacial alterations are obtained from MD simulation trajectories and averaged over the last 10 ns of the simulation time to ensure equilibrated values (see Fig. S5†). We tracked laponite–water, laponite–heptane and SDS–water interactions to probe the underlying intermolecular and interparticle energetics in the system as a function of SDS concentration. The interactions of laponite–water and laponite–heptane are normalized by the number of laponite nano-discs while the interactions of SDS–water are normalized by the number of SDS molecules dissolved in the heptane phase. The intermolecular interactions of laponite–water indicate that the suspension of laponite in water is mainly driven by electrostatic attractions while the contribution of van der Waals repulsion is minor. The magnitude of electrostatic interactions and van der Waals repulsion (the absolute values) increases systematically as the SDS concentration increases in the solution, suggesting stronger laponite–water interactions. The stronger interactions are driven by the displacement of interfacial laponite nano-discs from the interface toward the bulk aqueous phase which enables more bulk water molecules to interact with the nanoparticles stemming from the higher density of bulk water compared to interfacial water.

Further, the intermolecular interactions of laponite–heptane are insignificant compared to those in laponite–water systems (see Fig. S5(b)†). However, the change in these interactions as the SDS concentration increases confirms the interfacial transition from laponite-rich to SDS-rich interfaces. Electrostatic and van der Waals attractions contribute to the laponite-heptane interactions with slightly higher magnitudes of van der Waals. Both electrostatic and van der Waals interactions decrease systematically as the SDS concentration increases from 0 to 0.1 w%. The decrease in the laponite-heptane interactions suggests the laponite displacement from the interface as SDS molecules start occupying the interfacial area.

The interactions of SDS–water are mainly driven by the electrostatic attraction with a minor contribution of van der Waals attraction (see Fig. S5(c)†).[60] Interestingly, the SDS–water interactions show negligible dependency on the SDS concentration such that both electrostatic and van der Waals attractions remain relatively unchanged as the SDS concentrations increased from 0 to 0.1 wt%. These interaction profiles suggest the preferential adsorption of SDS molecules at the interface even at low SDS concentrations and the non-bonding interactions drive the alterationsdrive the alterations in the structural arrangement of laponite nano-discs and the rheological and nanomechanical properties of water–heptane interfaces.

4 Conclusions

In this study, a novel approach to direct the adsorption and assembly of 2D laponite nano-discs (diameter ~30 nm and thickness of ~1 nm) on water–heptane interfaces using small amounts of SDS surfactant molecules is developed, and the structural, rheological and nanomechanical properties of the interfaces using *in situ* USAXS/SAXS, AFM, SDT measurements and MD simulations are investigated. Perpendicular ('house of cards') and parallel ('stacked') arrangement of the laponite nano-discs are observed primarily due to the electrostatic interactions. The results show that the adsorption and assembly of interfacial laponite nano-discs can be reversed by introducing 0.1 wt% SDS that displaces the interfacial laponite nano-discs toward the bulk aqueous phase as SDS is a well-known electrostatic screening agent. The transition from a laponite-rich interface to an SDS-rich interface is associated with significant alterations in the rheological and nanomechanical properties of the interface. In this context, a reduction in the interfacial tension and interfacial stiffness and an increase in the interfacial deformation is observed upon the transition from laponite-rich to SDS-rich interfaces. The energetic analysis shows that the gradual laponite displacement which occurs as SDS molecules occupy the interfacial area is driven by the strong electrostatic interactions of the hydrophilic group in the SDS molecules with the interfacial water molecules. These insights are crucial for stimulating adsorption and assembly of 2D nanoparticles at water–hydrocarbon interfaces that are relevant to a wide range of scientific and technological applications including advanced materials synthesis such as emulsion stabilizers, nanopatterns, drug delivery vehicles, wastewater treatment, oil and gas recovery, and food processing.

Data availability

The data supporting this article have been included in the main manuscript and as part of the ESI.†

Conflicts of interest

There are no conflicts to declare for this work.

Acknowledgements

This work was supported as part of the Multi-Scale Fluid–Solid Interactions in Architected and Natural Materials (MUSE), an Energy Frontier Research Center funded by the U.S. Department of Energy, Office of Science, Basic Energy Sciences under Award # DE-SC0019285. This research used resources of the Advanced Photon Source; a U.S. Department of Energy (DOE) Office of Science user facility operated for the DOE Office of Science by Argonne National Laboratory under Contract No. DE-AC02-06CH11357. Ahmed Wasel Alsmaeil, Antonios Kouloumpis and Emannuel P. Giannellis acknowledge the support by the College of Petroleum Engineering and Geosciences, King Fahd University of Petroleum and Minerals. The authors also acknowledge Abdullah Aldariwish and Ziyad Alumair for their help in obtaining the interfacial tension measurements.

References

1 A. A. Umar, I. B. M. Saaid, A. A. Sulaimon and R. B. M. Pilus, *J. Pet. Sci. Eng.*, 2018, **165**, 673–690.
2 M. A. Hussein, A. A. Mohammed and M. A. Atiya, *Environ. Sci. Pollut. Res.*, 2019, **26**, 36184–36204.
3 R. J. Wilson, Y. Li, G. Yang and C.-X. Zhao, *Particuology*, 2022, **64**, 85–97.
4 F. Goodarzi and S. Zendehboudi, *Can. J. Chem. Eng.*, 2019, **97**(5), 281–309.
5 J. Smits, F. Vieira, B. Bisswurn, K. Rezwan and M. Maas, *Langmuir*, 2019, **35**, 11089–11098.
6 A. Barbul, K. Singh, L. Horev—Azaria, S. Dasgupta, T. Auth, R. Korenstein and G. Gompper, *ACS Appl. Nano Mater.*, 2018, **1**, 3785–3799.
7 H. Pei, J. Zheng, G. Zhang, J. Zhang and J. Zhao, *J. Mol. Liq.*, 2023, **376**, 121515.
8 H. Tomás, C. S. Alves and J. Rodrigues, *Nanomedicine*, 2018, **14**, 2407–2420.
9 H. Duan, D. Wang, D. G. Kurth and H. Möhwald, *Angew. Chem., Int. Ed.*, 2004, **43**, 5639–5642.
10 F. Reincke, W. K. Kegel, H. Zhang, M. Nolte, D. Wang, D. Vanmaekelbergh and H. Möhwald, *Phys. Chem. Chem. Phys.*, 2006, **8**, 3828–3835.
11 D. Wang, H. Duan and H. Möhwald, *Soft Matter*, 2005, **1**, 412.
12 B. J. Park and E. M. Furst, *Langmuir*, 2010, **26**, 10406–10410.
13 Y. Wang, C. Zhang, C. Tang, J. Li, K. Shen, J. Liu, X. Qu, J. Li, Q. Wang and Z. Yang, *Macromolecules*, 2011, **44**, 3787–3794.
14 I. Capek, *Adv. Colloid Interface Sci.*, 2004, **110**, 49–74.
15 K. Y. Lee, M. Kim, J. Hahn, J. S. Suh, I. Lee, K. Kim and S. W. Han, *Langmuir*, 2006, **22**, 1817–1821.
16 Z. Ye, C. Li, Q. Chen, Y. Xu and S. E. J. Bell, *Nanoscale*, 2021, **13**, 5937–5953.
17 S. Shi and T. P. Russell, *Adv. Mater.*, 2018, **30**(44), 1800714.
18 X.-C. Luu, J. Yu and A. Striolo, *Langmuir*, 2013, **29**, 7221–7228.
19 P. Y. Kim, Z. Fink, Q. Zhang, E. M. Dufresne, S. Narayanan and T. P. Russell, *ACS Nano*, 2022, **16**, 8967–8973.
20 D. Wang, Y.-L. Zhu, Y. Zhao, C. Y. Li, A. Mukhopadhyay, Z.-Y. Sun, K. Koynov and H.-J. Butt, *ACS Nano*, 2020, **14**, 10095–10103.
21 R. J. K. Udayana Ranatunga, R. J. B. Kalescky, C. Chiu and S. O. Nielsen, *J. Phys. Chem. C*, 2010, **114**, 12151–12157.
22 Y. Lin, H. Skaff, T. Emrick, A. D. Dinsmore and T. P. Russell, *Science*, 2003, **299**, 226–229.
23 M. G. Basavaraj, G. G. Fuller, J. Fransaer and J. Vermant, *Langmuir*, 2006, **22**, 6605–6612.
24 A. Böker, J. He, T. Emrick and T. P. Russell, *Soft Matter*, 2007, **3**, 1231.
25 J. Liu, G. Liu, M. Zhang, P. Sun and H. Zhao, *Macromolecules*, 2013, **46**, 5974–5984.
26 H. Tomás, C. S. Alves and J. Rodrigues, *Nanomedicine*, 2018, **14**, 2407–2420.
27 S. S. Das, Neelam, K. Hussain, S. Singh, A. Hussain, A. Faruk and M. Tebyetekerwa, *Curr. Pharm. Des.*, 2019, **25**, 424–443.
28 S. Wang, Y. Wu, R. Guo, Y. Huang, S. Wen, M. Shen, J. Wang and X. Shi, *Langmuir*, 2013, **29**, 5030–5036.
29 W. Li, L. Yu, G. Liu, J. Tan, S. Liu and D. Sun, *Colloids Surf., A*, 2012, **400**, 44–51.
30 N. P. Ashby and B. P. Binks, *Phys. Chem. Chem. Phys.*, 2000, **2**, 5640–5646.
31 J. Wang, G. Liu, L. Wang, C. Li, J. Xu and D. Sun, *Colloids Surf., A*, 2010, **353**, 117–124.
32 Y. Li, R. Zhao, F. Hu, P. Lu, D. Ji, Q. Luo, G. Li, D. Yu, H. Wang, Z. Song, S. Li and W. Liu, *Appl. Clay Sci.*, 2021, **206**, 106085.
33 Y. Yang, Z. Liu, D. Wu, M. Wu, Y. Tian, Z. Niu and Y. Huang, *J. Colloid Interface Sci.*, 2013, **410**, 27–32.
34 F. Li, L. Sun, Y. Wang, T. Wu and Y. Li, *J. Pet. Sci. Eng.*, 2014, **124**, 155–160.
35 C. Li, Q. Liu, Z. Mei, J. Wang, J. Xu and D. Sun, *J. Colloid Interface Sci.*, 2009, **336**, 314–321.
36 H. Wang, W. Liu, X. Zhou, H. Li and K. Qian, *Colloids Surf., A*, 2013, **436**, 294–301.
37 Q. Liu, S. Zhang, D. Sun and J. Xu, *Colloids Surf., A*, 2009, **338**, 40–46.
38 H. Machrafi, *npj Microgravity*, 2022, **8**, 47.
39 J. Smits, F. Vieira, B. Bisswurn, K. Rezwan and M. Maas, *Langmuir*, 2019, **35**, 11089–11098.

40 A. Barbul, K. Singh, L. Horev–Azaria, S. Dasgupta, T. Auth, R. Korenstein and G. Gompper, *ACS Appl. Nano Mater.*, 2018, **1**, 3785–3799.
41 S. Mohammed, I. Kuzmenko and G. Gadikota, *Nanoscale*, 2022, **14**, 127–139.
42 J. Ilavsky, P. R. Jemian, A. J. Allen, F. Zhang, L. E. Levine and G. G. Long, *J. Appl. Crystallogr.*, 2009, **42**, 469–479.
43 J. Ilavsky, F. Zhang, A. J. Allen, L. E. Levine, P. R. Jemian and G. G. Long, *Metall. Mater. Trans. A*, 2013, **44**, 68–76.
44 J. Ilavsky, *J. Appl. Crystallogr.*, 2012, **45**, 324–328.
45 J. Ilavsky and P. R. Jemian, *J. Appl. Crystallogr.*, 2009, **42**, 347–353.
46 J. D. Berry, M. J. Neeson, R. R. Dagastine, D. Y. C. Chan and R. F. Tabor, *J. Colloid Interface Sci.*, 2015, **454**, 226–237.
47 J. J. Kokelaar, A. Prins and M. De Gee, *J. Colloid Interface Sci.*, 1991, **146**, 507–511.
48 L. M. Daniel, R. L. Frost and H. Y. Zhu, *J. Colloid Interface Sci.*, 2007, **316**, 72–79.
49 L. Bippus, M. Jaber and B. Lebeau, *New J. Chem.*, 2009, **33**, 1116.
50 R. T. Cygan, J.-J. Liang and A. G. Kalinichev, *J. Phys. Chem. B*, 2004, **108**, 1255–1266.
51 H. J. C. Berendsen, J. R. Grigera and T. P. Straatsma, *J. Phys. Chem.*, 1987, **91**, 6269–6271.
52 W. L. Jorgensen, D. S. Maxwell and J. Tirado-Rives, *J. Am. Chem. Soc.*, 1996, **118**, 11225–11236.
53 S. Nosé, *Mol. Phys.*, 1984, **52**, 255–268.
54 W. G. Hoover, *Phys. Rev. A*, 1985, **31**, 1695–1697.
55 M. Parrinello and A. Rahman, *J. Chem. Phys.*, 1982, **76**, 2662–2666.
56 T. Darden, D. York and L. Pedersen, *J. Chem. Phys.*, 1993, **98**, 10089–10092.
57 M. J. Abraham, T. Murtola, R. Schulz, S. Páll, J. C. Smith, B. Hess and E. Lindahl, *SoftwareX*, 2015, **1–2**, 19–25.
58 C. Vashisth, C. P. Whitby, D. Fornasiero and J. Ralston, *J. Colloid Interface Sci.*, 2010, **349**, 537–543.
59 B. Jönsson, C. Labbez and B. Cabane, *Langmuir*, 2008, **24**, 11406–11413.
60 G. Beaucage and D. W. Schaefer, *J. Non-Cryst. Solids*, 1994, **172–174**, 797–805.
61 T. Li, A. J. Senesi and B. Lee, *Chem. Rev.*, 2016, **116**, 11128–11180.
62 T. Suzuki, A. Chiba and T. Yarno, *Carbohydr. Polym.*, 1997, **34**, 357–363.
63 E. Rio, W. Drenckhan, A. Salonen and D. Langevin, *Adv. Colloid Interface Sci.*, 2014, **205**, 74–86.
64 D. Bonn, S. Tanase, B. Abou, H. Tanaka and J. Meunier, *Phys. Rev. Lett.*, 2002, **89**, 015701.
65 A. Shahin and Y. M. Joshi, *Langmuir*, 2010, **26**, 4219–4225.
66 R. M. Guillermic, A. Salonen, J. Emile and A. Saint-Jalmes, *Soft Matter*, 2009, **5**, 4975.
67 H.-Q. Sun, L. Zhang, Z.-Q. Li, L. Zhang, L. Luo and S. Zhao, *Soft Matter*, 2011, **7**, 7601.
68 J. Saien and M. Bahrami, *J. Mol. Liq.*, 2016, **224**, 158–164.
69 H. Ma, M. Luo and L. L. Dai, *Phys. Chem. Chem. Phys.*, 2008, **10**, 2207.
70 J. T. Russell, Y. Lin, A. Böker, L. Su, P. Carl, H. Zettl, J. He, K. Sill, R. Tangirala, T. Emrick, K. Littrell, P. Thiyagarajan, D. Cookson, A. Fery, Q. Wang and T. P. Russell, *Angew. Chem.*, 2005, **117**, 2472–2478.
71 J. G. Parra, H. Domínguez, Y. Aray, P. Iza, X. Zarate and E. Schott, *Colloids Surf., A*, 2019, **578**, 123615.
72 N. Choudhary, A. K. Narayanan Nair and S. Sun, *Soft Matter*, 2021, **17**, 10545–10554.
73 C. D. Bruce, S. Senapati, M. L. Berkowitz, L. Perera and M. D. E. Forbes, *J. Phys. Chem. B*, 2002, **106**, 10902–10907.
74 S. Velioğlu, L. Han and J. W. Chew, *J. Membr. Sci.*, 2018, **551**, 76–84.